Superlattices and Microstructures 136 (2019) 106309

Contents lists available at ScienceDirect

Superlattices and Microstructures

journal homepage: www.elsevier.com/locate/yspmi

Relationship between the ideality factor and the iron concentration in silicon solar cells

O.Ya. Olikh

Faculty of Physics, Taras Shevchenko National University of Kyiv, Kyiv 01601, Ukraine

ARTICLE INFO

Keywords:
Silicon solar cell
SCAPS simulator
Ideality factor
Iron concentration

ABSTRACT

The ideality factor value of silicon $n^+ - p$ solar cells with iron contaminants has been studied by means of computer simulation. The iron concentration range of $10^{10} - 10^{13}$ cm^{-3}, base doping level range of $10^{15} - 10^{17}$ cm^{-3}, and temperature range of 290 – 340 K were used in the investigation. The Solar Cells Capacitance Simulator (SCAPS) was the tool used for numerical simulation of these devices. The two-diode model was used to extract the ideality factor. The following cases were considered: (i) Shockley–Read–Hall (SRH) recombination; (ii) both intrinsic recombination and SRH recombination; (iii) unpaired interstitial iron atoms; (iv) both iron–boron pairs and interstitial iron atoms. The algorithms of iron concentration evaluation in silicon solar cell by using current–voltage curve are proposed. The analytic expressions are suggested as well as calibration curves are calculated.

1. Introduction

It is well known that impurities are crucial for semiconductor device performance, which is completely relevant to the solar cell (SC) too. The dopants determinate internal electric field, which leads to the separation of light-generated carriers and generation of photoelectric voltage. The contaminants often act as highly effective recombination centers, which reduces the carrier lifetime and SC efficiency. Therefore, it is very important to estimate the impurity concentration. There are many experimental methods for solving this problem, such as the infrared spectroscopy, deep level transient spectroscopy, photoluminescence, thermally stimulated capacitance and current, secondary ion mass spectrometry etc [1]. These methods are complicated enough and demand a special setup.

At the same time, there is a simpler and more commonly used technique, which is the analysis of the solar cell current–voltage ($I - V$) characteristics. In particular, a dark $I - V$ curve normally serves as the first diagnosis of SC recombination [2]. The $I - V$ equation, which models the SC by equivalent electrical circuit, contains several parameters related to the physical phenomena that occur in the device. It is obvious that these parameters depend on impurities, but the interrelations are sufficiently intricate. As a result, the $I - V$ curves are not used in practice to estimate contaminants, although the possibility to calibrate simultaneously both SC performance and impurities looks quite attractive.

One of a number of parameters of SC model is the ideality factor n. The value of $n > 1$ indicates that the carrier recombination mechanism in the solar cell involves traps. If the defect related recombination is dominant, the value often reported in publications is $n = 2$. This value, however, suggests very specific assumptions about the energy levels (the middle part of the bandgap) and capture cross sections of the recombination centers (which are the same both for electrons and holes) in the symmetrically doped diode [3,4]. Typically, the value of the ideality factor ranges from 1 to 2 for real devices and depends on ambient conditions and

E-mail address: olikh@univ.kiev.ua.

https://doi.org/10.1016/j.spmi.2019.106309
Received 10 September 2019; Received in revised form 13 October 2019; Accepted 15 October 2019
Available online 17 October 2019

Table 1
Temperature dependencies of basic material parameters used in the simulation.

Material properties	Symbol	Value	Ref.
Bandgap (eV)	E_g	$1.169-\frac{7.021\times10^{-4}T^2}{(T+1108)}$	[1]
Bandgap narrowing (meV)	ΔE_g	$6.92\cdot\left[\ln\left(\frac{N_D+N_A}{1.3\times10^{17}}\right)+\sqrt{\left(\ln\left(\frac{N_D+N_A}{1.3\times10^{17}}\right)\right)^2+\frac{1}{2}}\right]$	[22,23]
Effective density of states at			
- conduction band (cm^{-3})	N_C	$2.86\times10^{19}\left(\frac{T}{300}\right)^{1.58}$	[24]
- valence band (cm^{-3})	N_V	$3.1\times10^{19}\left(\frac{T}{300}\right)^{1.85}$	[24]
Thermal velocity of			
- electron (m/s)	$\upsilon_{th,n}$	$\sqrt{\frac{8qkT}{0.28m_0\pi}}$	[24]
- hole (m/s)	$\upsilon_{th,p}$	$\sqrt{\frac{8qkT}{0.41m_0\pi}}$	[24]
Mobility of			
- electron (cm^2/V s)	μ_n	$92\left(\frac{T}{300}\right)^{-0.57}+\frac{1268\left(\frac{T}{300}\right)^{-2.33}}{1+\left[\frac{N_D}{1.3\times10^{17}\left(\frac{T}{300}\right)^{2.4}}\right]^{\zeta_n}}$, $\zeta_n=0.91\left(\frac{T}{300}\right)^{-0.146}$	[1]
- hole (cm^2/V s)	μ_p	$54.3\left(\frac{T}{300}\right)^{-0.57}+\frac{407\left(\frac{T}{300}\right)^{-2.23}}{1+\left[\frac{N_A}{2.35\times10^{17}\left(\frac{T}{300}\right)^{2.4}}\right]^{\zeta_p}}$, $\zeta_p=0.88\left(\frac{T}{300}\right)^{-0.146}$	[1]
Recombination coefficient			
- Auger, electron (cm^6/s)	C_n	2.8×10^{-31}	[22]
- Auger, hole (cm^6/s)	C_p	9.9×10^{-32}	[22]
- radiative (cm^3/s)	B	1.8×10^{-15}	[22]

recombination center parameters, including the concentration of traps [4–8]. This makes the ideality factor an important parameter that can be used to describe the electrical behavior of photovoltaic devices and characterize the recombination in SCs [9].

The aim of our work is to apply the ideality factor for evaluating the contaminant concentration. In the heuristic approach we use, the following milestones can be distinguished (i) the dark $I-V$ characteristic is simulated for SCs with known contaminant composition; (ii) the obtained characteristic is fitted according to the double-diode model and the ideality factor is estimated; (iii) the initial impurity concentration and the calculated ideality factor value are used for deriving analytic or grading dependencies.

As the first approximation, the paper considers a fairly simple system which is, however, important in practice. The system consists of crystalline silicon SC and iron impurity. Si photovoltaic devices cover almost 90% of global SC market. Iron is a major contaminant, which is due to the wide use of stainless steel equipment in the fabrication line, as well as one of the most detrimental metal impurities in solar-grade crystalline silicon materials [10–12].

In our numerical simulation we make use of one-dimensional code SCAPS [13,14].

This software is widely applied in modeling various solar cells [15–21], silicon based devices including [19–21].

2. Simulation details

The calculation presented here uses simple n^+-p structure shown in inset in Fig. 2. The initial thickness of each layer $d_n = 0.5$ μm and $d_p = 300$ μm respectively; n^+ is the emitter layer with the donor concentration $N_D = 10^{19}$ cm^{-3} and $10^{15}-10^{17}$ cm^{-3} is the acceptor concentration N_A of the p base layer, which is uniformly doped with boron.

The simulations were carried out over the temperature range $290-340$ K. It should be noted that SCAPS only takes into account the simplified temperature dependencies of density of states and thermal velocity of carriers. Therefore the SCAPS setting file was created for each temperature using the material and defect parameters of Tables 1 and 2 respectively.

As the base layer uniform contaminant, iron is assumed to be in concentration $10^{10}-10^{13}$ cm^{-3}. Iron atoms are known to be predominantly located in interstitial lattice position in silicon and the donor level $E_{Fe_i} = E_V + 0.394$ eV is associated with Fe_i [25,26]. Therefore, the iron in Si is neutral Fe_i^0 and ionized Fe_i^+ interstitial. In p–type material, Fe_i^+ readily interacts with ionized shallow acceptors. So in our simulation, we should consider the pair Fe_iB_s. On the one hand, this pair is a bistable defect and the trigonal and orthorhombic configurations are feasible. On the other hand, the orthorhombic pair is only observable at low temperature (<150 K)

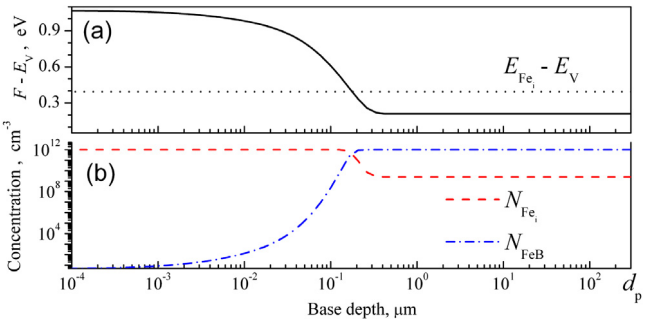

Fig. 1. The calculated SC base distribution of Fermi level position (a, solid line), unpaired interstitial iron concentration (b, dashed line), and Fe_iB_s pair concentration (b, dotted–dashed line). $N_A = 10^{16}$ cm^{-3}, $T = 300$ K. The position of Fe_i donor level (dotted line) is shown in the panel (a) as well.

Table 2
The parameters of the impurity centers taken from [10,25,26,29] and used in the calculation.

Defect type	Fe_i	Fe_iB_s	
Level type	Donor	Donor	Acceptor
Energy level (eV)	$E_V + 0.394$	$E_V + 0.10$	$E_C - 0.26$
σ_n (cm^2)	$9.1 \times 10^{-15} \exp(-\frac{0.024}{kT})$	4×10^{-13}	2.5×10^{-15}
σ_p (cm^2)	$3.85 \times 10^{-16} \exp(-\frac{0.045}{kT})$	2×10^{-14}	5.5×10^{-15}

under illumination or in the conditions of carrier injection [27,28]. Besides, the Fe_iB_s pairs can be readily dissociated by 15 to 90 s illumination with a halogen lamp [11]. The association reaction is diffusion limited and can take place when exposed in darkness for ten minutes [29].

The simulations have been performed for the following two cases.

(i) The assumption about negligible portion of Fe available in the form of Fe_iB_s pairs:

$$N_{Fe} = N_{Fe_i^0} + N_{Fe_i^+}, \tag{1}$$

where $N_{Fe_i^0}$ and $N_{Fe_i^+}$ are the concentrations of neutral and ionized iron respectively. This is a safe assumption for solar cell operation under constant illumination or immediately after its termination. The hole σ_p and electron σ_n capture cross-sections of defect are calculated according to Table 2 data. E_{Fe_i} is taken as the temperature independent value [30]. This case is labeled "FI" from now on.

(ii) The assumption about equilibrium condition when the concentration of totally dissolved iron is given by a sum of concentrations of three separate species

$$N_{Fe} = N_{Fe_i^0} + N_{Fe_i^+} + N_{FeB}, \tag{2}$$

where N_{FeB} is the Fe_iB_s pair concentration. By using the relationships between the equilibrium concentration of Fe_i^+, Fe_i^0, and Fe_iB_s from [26,29] we obtain the following expression

$$N_{FeB} = N_{Fe} \frac{N_A 10^{-23} \exp\left(-\frac{E_b}{kT}\right)}{\left[1 + N_A 10^{-23} \exp\left(-\frac{E_b}{kT}\right)\right]\left[1 + \exp\left(-\frac{F - E_{Fe_i}}{kT}\right)\right]}. \tag{3}$$

where F is the Fermi level, E_b is the binding energy of the Fe_iB_s pairs (taken as 0.582 eV). Hence it should be taken under account that the distribution of Fe_iB_s pair is uniform. In our simulation, first, the Fermi level position in the base layer is calculated for each doping level as well as for each temperature. Then, Eq. (3) is used to calculate the Fe_iB_s pair distribution. The representative example of calculation is shown in Fig. 1.

In our work we considered the trigonal Fe_iB_s pair, which is a true condition at room temperature. This pair is amphoteric defect and its parameters are listed in Table 2. Here ad further on, this case is labeled "FIFB".

In this paper, we analyze only bulk recombination, and again two cases are simulated. In the first one, labeled "SRH", the Shockley–Read–Hall recombination is taken into account only. In the second one, denoted "SRHBBA", the both Shockley–Read–Hall recombination and intrinsic recombination are allowed.

Thus, four different data sets (FI-SRH, FI-SRHBBA, FIFB-SRH, and FIFB-SRHBBA) have been chosen to simulate solar cell.

The dark forward $I - V$ characteristic were generated by SCAPS over a voltage range up to 0.62 V. The example of $I - V$ curve is shown in Fig. 2.

The real silicon SCs are often described by the so-called two-diode model [31]. The first diode represents the "ideal" diode, describing the so-called diffusion current characterized by a saturation current I_{01}, and the second diode is the so-called

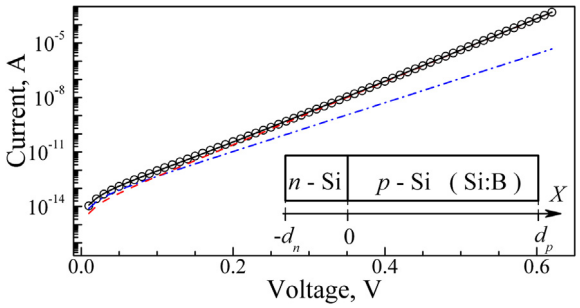

Fig. 2. $I-V$ characteristic simulated in FI-SRH-case, $N_A = 10^{17}$ cm^{-3}, $N_{Fe} = 10^{13}$ cm^{-3}, $T = 290$ K (marks) and its fitting by Eq. (4) (solid line). The dashed and dotted–dashed lines represent the diffusion and recombination currents. Inset: Solar cell structure, which are used in simulation.

recombination current, characterized by the saturation current I_{02} and ideality factor n [31]. According to the two-diode model, the dark SC current is given by

$$I = I_{01}\left[\exp\left(-\frac{qV}{kT}\right)-1\right] + I_{02}\left[\exp\left(-\frac{qV}{nkT}\right)-1\right]. \tag{4}$$

It should be noted that the influence of series resistance as well as shunt resistance is neglected in Eq. (4). We used Eq. (4) to fit the simulated data by taking n, I_{01}, and I_{02} as fitting parameters. The fitting was performed by using the differential evolution (DE) algorithm [32,33]. DE is a population-based stochastic optimization technique that can be applied to solve global optimization problems [34]. DE based on the natural selection law and used the random generated initial population, differential mutation, and probability crossover. In our case the population consist of sets of 3 parameters $\{I_{01}, I_{02}, n\}$ to be found. Three main control parameters of differential evolution are the population size NP, mutation factor F, and the crossover rate CR. According to Wang and Ye [33], the values $F = 0.8$, $CR = 0.3$, and $NP = 24$ are used in this work. The used fitness function can be given by

$$Fit = \sum_{i=1}\left\{1 - \frac{I_{01}}{I_i}\left[\exp\left(-\frac{qV_i}{kT}\right)-1\right] + \frac{I_{02}}{I_i}\left[\exp\left(-\frac{qV_i}{nkT}\right)-1\right]\right\}^2, \tag{5}$$

where V_i and I_i are the coordinates of i–th point of the simulated I–V curve.

The result of the fitting is shown in Fig. 2. It is the ideality factor value which is used in our further analysis.

DE was used to other non-linear fittings as well.

3. Results and discussion

3.1. Interstitial iron, SRH recombination

A number of data calculated for the FI-SRH case are shown in Fig. 3(a,b). It is seen that the ideality factor increases monotonically as the doping level increases. However, temperature dependence of n is more intricate: it contains both increasing and decreasing components, and the contribution of the latter rises with the increase in N_A. The growth of iron concentration leads to the increase in n value, while $n(N_A, T)$ dependence does not change — see Fig. 3 and Supplementary Material. This is the evidence of possibility to evaluate N_{Fe} by using n. Only low doping level value ($N_A \cong 10^{15}$ cm^{-3}) and high temperature ($T > 300$ K) are exclusions because according to the simulation results, n is approximately equal to 1.

It is obvious that an analytical expression would be more convenient for evaluating N_{Fe}. To derive an expression of this kind, the fact that the interstitial iron captures an electron in p–type silicon should be taken into account. Therefore, the recombination efficiency is determined by a hole occurring on the Fe_i level. The probability of hole occupation is $f_p = \left[1+\exp\left(\frac{F-E_{Fe_i}}{kT}\right)\right]^{-1}$ and this equation can be a starting point to build the expression $n = n(T, N_A, N_{Fe})$. It should be noted that, unlike the simulated $n(N_A, T)$ relationship, $f_p(N_A, T)$ depends on temperature monotonically and reaches saturation with the increase in N_A — see Supplementary Material. In addition, the Fermi level can be evaluated by the equation $(F - E_V) = kT\ln(N_V/N_A)$ under the conditions of the given simulation.

Basing on the above considerations, we search for expression $n = n(T, N_A, N_{Fe})$ in the following form:

$$n(T, N_A, N_{Fe}) = 1 + \frac{n_0(N_{Fe})\cdot T^{m_T}\cdot(\log N_A)^{m_A}}{1 + N_V(T)\cdot\gamma(N_A, N_{Fe})\cdot\exp\left(\frac{E_{ef}(T,N_A)}{kT}\right)}, \tag{6}$$

where m_T and m_A are the power exponents of temperature dependence and doping level dependence respectively; n_0 and γ are the pre-factors of ideality factor and Fermi level respectively; E_{ef} is the effective energy of defect level. In fitting, m_T and m_A are the constant, and fitness parameters n_0, γ, and E_{ef} depend on iron concentration, doping level, and temperature.

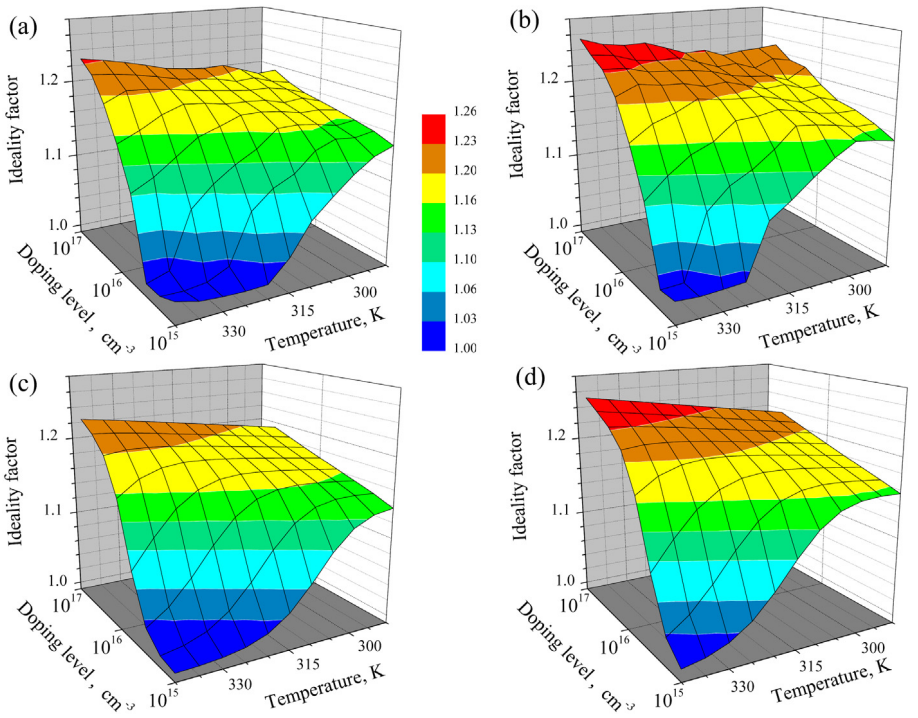

Fig. 3. Ideality factor as a function of the temperature and dopant (boron) concentration. FI-SRH case. N_{Fe}, cm^{-3}: 10^{10} (a,c), 10^{13} (b,d). The simulated data are in panels (a) and (b); the fittings of simulated data with help Eq. (6) are in panels (c) and (d).

Table 3
Fitting parameters in Eq. (6) of simulated dependencies of ideality factor.

Simulation case	Parameter			
	m_T	m_A	γ (cm^3)	E_{ef} (eV)
FI-SRH	1.13	2.85	N_A^{-1}	$1.43-\frac{0.085\,T}{\log N_A}+0.0019\,T$
FI-SRHBBA	1.3	2.85	Eq. (10)	$9.53-0.52\log N_A$
FIFB-SRH	2.2	2.85	Fig. 9(a)	$16.6-0.90\log N_A$
FIFB-SRHBBA	2.2	2.85	Fig. 9(b)	$13.4-0.77\log N_A$

m_T Power exponent of temperature dependence.
m_A Power exponent of doping level dependence.
γ Pre-factors of Fermi level.
E_{ef} Effective energy of defect level.

The analysis has shown that the simulated data are well fitted by Eq. (6) with $m_T = 1.13$, $m_A = 2.85$, $\gamma = N_A^{-1}$ and the dependence of the effective energy E_{ef} can be expressed as:

$$E_{ef}(T, N_A) = E_0 - \alpha T/\log N_A + \beta T\,, \tag{7}$$

where values $E_0 = 1.43 \pm 0.08$ eV, $\alpha = 85 \pm 5$ meV cm^{-3} K^{-1}, and $\beta = 1.9 \pm 0.2$ meV K^{-1} do not depend on N_{Fe} practically. The parameters are listed in Table 3 and the results of the fitting are shown in Fig. 3(c,d) and Supplementary Material. A good agreement of simulated data and fitting curves prove the expediency of Eq. (6) use. It is interesting, that the obtained value of $m_T = 1.13$ is very close to the value of 1.1368 of power exponent of temperature dependence of ideality factor, which has been early determined for silicon photovoltaic module by Siddiqui et al. [35]

Thus, in the FI-SRH case, the simulated (semi-empirical) dependence of the ideality factor takes the following shape:

$$n = 1 + \frac{n_0(N_{Fe})\cdot T^{1.13}\cdot(\log N_A)^{2.85}}{1+\frac{N_V(T)}{N_A}\cdot\exp\left(\frac{1.43}{kT}-\frac{986}{\log N_A}+22\right)}\,. \tag{8}$$

We use Eq. (8) by taking n_0 as fitting parameter to fit the n dependencies calculated for different N_{Fe} values. The resulting n_0 dependence on iron concentration is shown in Fig. 4. This curve is monotonic as well as smooth enough and can serves as a

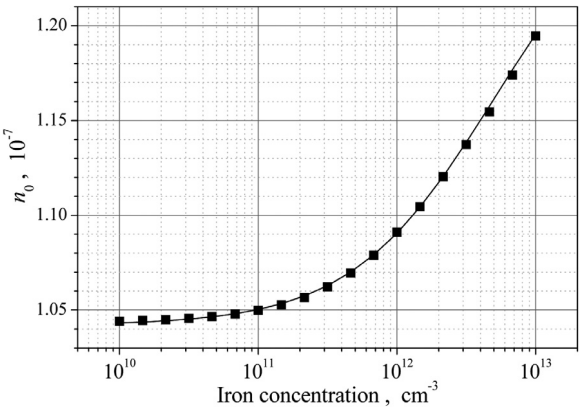

Fig. 4. Dependence of the parameter n_0 (see Eq. (6)) on the iron concentration in SC base. FI-SRH case. Line is the fitted curve using Eq. (9).

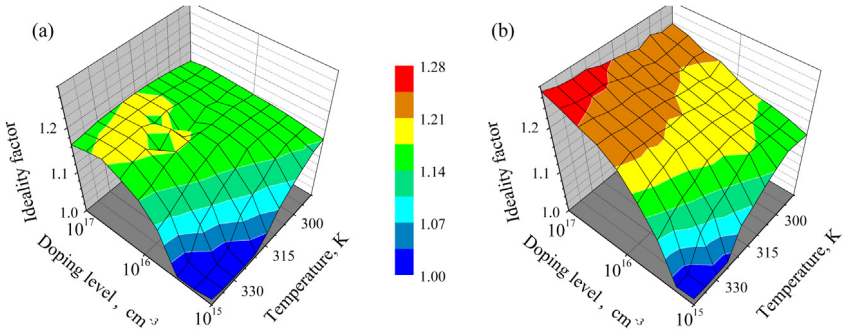

Fig. 5. Ideality factor as a function of the temperature and dopant (boron) concentration. FI-SRHBBA case. N_{Fe}, cm^{-3}: 10^{10} (a), 10^{13} (b).

calibration curve. In addition, the found dependence is well described by Eq. (9):

$$n_0(N_{Fe}) = 1.28\times10^{-7} - \frac{2.38\times10^{-8}}{1+\left(\frac{N_{Fe}}{4.96\times10^{12}}\right)^{0.85}}. \tag{9}$$

Thus, the algorithm of iron concentration evaluation in silicon SC by using a $I-V$ curve can be as follows.

(i) The solar cell is illuminated by 15 to 90 s with a halogen lamp to dissociate the FeB pairs. When illumination is terminated, the $I-V$ characteristic is measured.
(ii) $I-V$ curve is fitted accordingly to the two-diode model and the ideality factor n is determined.
(iii) Taking into account n value, doping level N_A, and measurement temperature, the parameter n_0 is calculated by relationship

$$n_0 = (n-1)\cdot\frac{1+\frac{N_V(T)}{N_A}\cdot\exp\left(\frac{1.43}{kT}-\frac{986}{\log N_A}+22\right)}{T^{1.13}\cdot(\log N_A)^{2.85}}.$$

(iv) N_{Fe} is evaluated by using the calibration curve in Fig. 4 or by the following expression

$$N_{Fe} = 4.96\times10^{12}\cdot\left(\frac{2.38\times10^{-8}}{1.28\times10^{-7}-n_0}\right)^{1.18}.$$

3.2. Interstitial iron, SRH recombination, intrinsic recombination

It should be noted that the above algorithm undergoes modifications when Auger recombination and band-to-band recombination are taken into account. In fact, the simulation show that the dependencies $n(N_A,T)$ are partially changed — see Fig. 5. It is quite expectable that these changes grow with the N_A increase and N_{Fe} decrease. Besides, the non-monotonic dependencies $n(N_A,T)$ are observed at low iron concentration. Thus, the search for analytical expression qualified for each value of temperature and doping level seems inappropriate.

On the other hand, since room temperature measurements of $I-V$ characteristics alone cannot provide the detailed information about the SC properties; additional insight is often gained by characterizing the devises over a certain temperature range. Therefore

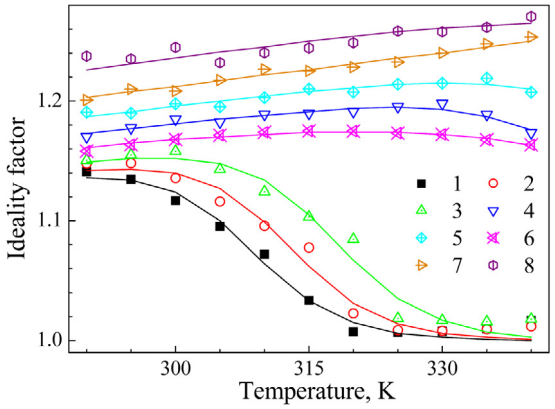

Fig. 6. Temperature dependencies of the ideality factor. FI-SRHBBA case. The marks are the simulation results, and the lines are the fitted curves using Eq. (6) and data in Table 3. N_{Fe}, cm^{-3}: 10^{10} (curves 1, 6), 10^{12} (2, 4, and 7), 10^{13} (3, 5, and 8). N_A cm^{-3}: 10^{15} (1, 2, and 3), 10^{16} (4, 5), 10^{17} (6, 7, and 8).

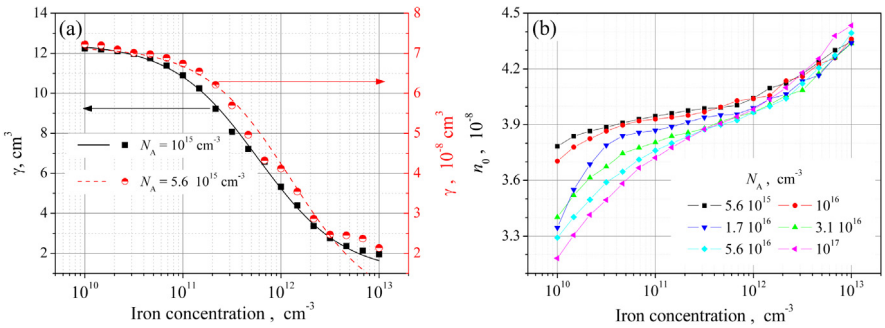

Fig. 7. Dependencies of the parameters γ (a) and n_0 (b) on the iron concentration in SC base. FI-SRHBBA case. Lines in panel (a) are the fitted curves using Eq. (10), lines in panel (b) only serve as guide to the eye.

in this case, we try to evaluate iron concentration by using the temperature dependence of the ideality factor, which is measured (simulated) for the solar cell with the known constant doping level — $n(T)@N_A$.

Some of the obtained curves $n(T)$ are shown in Fig. 6. One can see that the N_A value affects substantively the temperature dependence of the ideality factor. We use Eq. (6) and $m_A = 2.85$ to fit the simulated $n(T)@N_A$. A close agreement between simulated and fitted data has been found by using $m_T = 1.3$ and $E_{ef} = (9.53 - 0.52 \log N_A)$ — see lines in Fig. 6.

The values of other parameters n_0 and γ depend on doping level as well as iron concentration and can be used to evaluate N_{Fe}. Thus, as shown in Fig. 7(a), the dependencies $\gamma(N_{Fe})$ can be described by the following equation:

$$\gamma = \left(\frac{10^{15}}{N_A}\right)^{11} \cdot \frac{\eta N_0 + N_{Fe}}{N_0 + N_{Fe}}. \tag{10}$$

where $10 \div 15$ and $(0.5 \div 1) \times 10^{12}$ cm^{-3} are the η and N_0, respectively at various boron concentrations.

The concentration dependencies of the parameter n_0 are shown in Fig. 7(b) and can serve as calibration curves as well. As seen from the figure, for a high base doping level ($N_A > 10^{16}$ cm^{-3}), the evaluation of iron concentration by using the n_0 value is advisable. At a low N_A value, the weak dependence n_0 on N_{Fe} impairs the estimation accuracy. Simultaneously, the opposite case is observed for parameter γ and it is better to evaluate N_{Fe} by the γ value at a low doping level, otherwise the γ decreases significantly (see Eq. (10)) and the accuracy of γ evaluation by Eq. (6) fitting becomes much lower.

3.3. Iron–boron pair and interstitial iron

The results obtained under equilibrium condition in the presence of Fe_iB_s are illustrated by Fig. 8. The main features of the ideality factor variations are actually in agreement with the case of the SC free from Fe_iB_s contaminant. Namely, n increases with the increase in N_{Fe}, the $n(T)$ dependence is non-monotonic, which pronounced with decrease in N_A, etc. First of all, this happens because Fermi level is far from the valence band, the neutral interstitial Fe_i^0 is dominant, and the boron containing complex is not created within a space charge region (SCR) — see Fig. 1. That is, in contrast with the quasi neutral region, the illumination does not cardinally change the N_{Fe_i} and $N_{Fe_iB_s}$ ratio. At the same time, the value of ideality factor is affected mainly by the SCR recombination. However, the n absolute value is smaller in FIFB-case then that in the FI-case, because Fe_i and Fe_iB_s have different

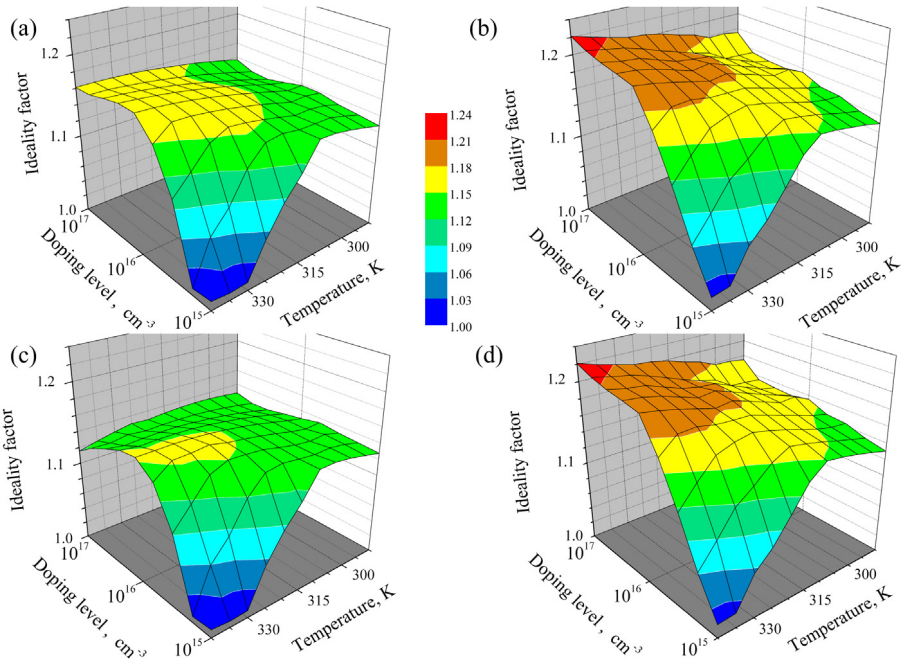

Fig. 8. Ideality factor as a function of the temperature and dopant (boron) concentration. FIFB-SRH (a,b) and FIFB-SRHBBA (c, d) cases. N_{Fe}, cm^{-3}: 10^{10} (a, c), 10^{13} (b, d).

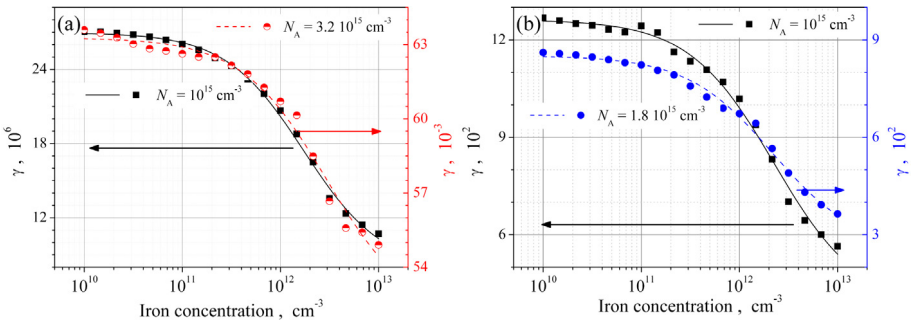

Fig. 9. Dependencies of the parameters γ on the iron concentration in SC base. FIFB-SRH (a) and FIFB-SRHBBA (b) cases. Lines are the fitted curves using Eq. (10).

energy levels and cross-sections for recombination. The comparison of Fig. 8(a) and (c) as well as Fig. 8(b) and (d) shows that the intrinsic recombination affects the n value at low iron concentration, high temperature, and high doping level.

Similar to the previous FI-SRHBBA case, different $n(N_A, T)$ dependencies are observed at the different values of N_{Fe}. Like in the previous case, we consider the temperature dependencies of ideality factor $n(T)@N_A$ and use Eq. (6) to fit the simulated data. The simulated data have been found to be in good agreement with the fitting curves (see Supplementary Material) for values $m_T = 2.2$ and E_{ef}, which are linear dependent of $\log N_A$. The data are given in Table 3.

The obtained dependencies of parameters γ and n_0 on iron concentration are shown in Figs. 9 and 10 respectively and can serve as calibration curves as well. Again, it is more appropriate to use the parameter γ for N_{Fe} evaluation at low boron concentrations and the parameter n_0 in the opposite case. However, the conditional limit shifts toward the smaller N_A values and comprises about 3×10^{15} cm^{-3}. In this case, the main difference between calibration curves in the FIFB-SRH and FIFB-SRHBBA cases is also observed for $N_{Fe} < 10^{11}$ cm^{-3} and $N_A > 3\times10^{16}$ cm^{-3}.

Thus, another, more complicated but more general, algorithm of an iron concentration evaluation can be offered.

(i) The dark $I - V$ characteristics of the silicon SC are measured over the temperature range of about 290 – 340 K. The measurements can be carried out after a halogen lamp illumination or after a long-term storing in the dark.
(ii) $I - V$ curves are fitted accordingly to the two-diode model and the temperature dependency of the ideality factor $n(T)$ is determined.

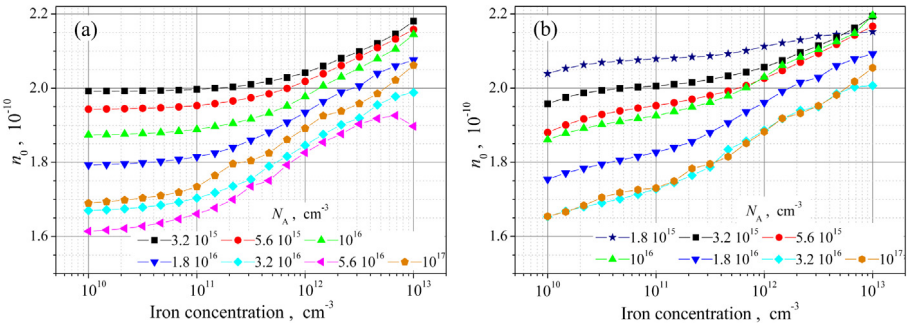

Fig. 10. Dependencies of the parameters n_0 on the iron concentration in SC base. FIFB-SRH (a) and FIFB-SRHBBA (b) cases. Lines only serve as guide to the eye.

(iii) Eq. (6) and Table 3 are used to fit the $n(T)$. The n_0 and γ are taken as the fitting parameters.
(iv) N_{Fe} is evaluated by using calibration curves in Fig. 7 or in Figs. 9(b) and 10(b) after illumination or dark storing measurements, respectively.

4. Conclusion and outlook

The relationship between the diode ideality factor and the iron concentration in the base layer of silicon $n^+ - p$ solar cells has been studied via computer simulation. The data used in the simulations were the following. The iron concentration ranged from 10^{10} to 10^{13} cm^{-3}, the base doping level — from 10^{15} to 10^{17} cm^{-3}, and the temperature — from 290 to 340 K. The obtained results show that the ideality factor value can be used to estimate the contaminant concentration. In particular, the analysis has shown that in case of the Shockley–Read–Hall recombination and the unpaired interstitial iron, it is sufficient to measure single $I - V$ characteristic measurement and find single ideality factor value to evaluate iron concentration. If the Auger recombination, radiative recombination, or iron–boron pair presence has to be taken into account, then the measurements over a temperature range are necessary. For these cases, we have calculated the calibration curves and suggested analytic expressions.

However, it should be noted that we have simplified the task for our purposes and the set of variables consists only of three values (temperature, doping level, and iron concentration). The obtained analytical expression is supposed to be used only for approximation case. As shown by the simulation, the geometry of the solar cell (e.g. base layer thickness) also affects the magnitude of ideality factor. In general case, the ideality factor can be used to estimate not only a trap concentration but also the energy level and capture cross-section. This multivariable problem would involve a huge set of calibration curves and as an option, the artificial neural networks would be very efficient.

Declaration of competing interest

The authors declare that they have no known competing financial interests or personal relationships that could have appeared to influence the work reported in this paper.

Appendix A. Supplementary data

Supplementary material related to this article can be found online at https://doi.org/10.1016/j.spmi.2019.106309.

References

[1] D.K. Schroder, Semiconductor Material and Device Characterization, third ed., John Wiley & Sons, New Jersey, 2006.
[2] S. Grover, A.J.V. Li, D.L. Young, P. Stradins, H.M. Branz, Reformulation of solar cell physics to facilitate experimental separation of recombination pathways, Appl. Phys. Lett. 103 (9) (2013) 093502, http://dx.doi.org/10.1063/1.4819728.
[3] R. Kuhn, P. Fath, E. Bucher, Effects of pn–junctions bordering on surfaces investigated by means of 2D–modeling, in: Conference Record of the Twenty–Eighth IEEE Photovoltaic Specialists Conference – 2000 (Cat. No.00CH37036), 2000, pp. 116–119, http://dx.doi.org/10.1109/PVSC.2000.915768.
[4] J. Beier, B. Voss, Humps in dark I–V–curves–analysis and explanation in: Conference Record of the Twenty Third IEEE Photovoltaic Specialists Conference - 1993 (Cat. No.93CH3283-9), 1993, pp. 321–326, http://dx.doi.org/10.1109/PVSC.1993.347163.
[5] K. McIntosh, P. Altermatt, G. Heiser, Depletion–region recombination in silicon solar cells. When does $mdr = 2$? in: 16th European Photovoltaic Solar Energy Conference: Proceedings of the International Conference and Exhibition, James and James (Science Publishers) Ltd, 2000, pp. 250–253.
[6] A. Kaminski, J.J. Marchand, H. El Omari, A. Laugier, Q.N. Le, D. Sarti, Conduction processes in silicon solar cells, in: Conference Record of the Twenty Fifth IEEE Photovoltaic Specialists Conference – 1996, 1996, pp. 573–576, http://dx.doi.org/10.1109/PVSC.1996.564071.
[7] Z. Hameiri, K. McIntosh, G. Xu, Evaluation of recombination processes using the local ideality factor of carrier lifetime measurements, Sol. Energy Mater. Sol. Cells 117 (2013) 251–258, http://dx.doi.org/10.1016/j.solmat.2013.05.040.
[8] A.S.H. van der Heide, A. Schonecker, J.H. Bultman, W.C. Sinke, Explanation of high solar cell diode factors by nonuniform contact resistance, Prog. Photovolt., Res. Appl. 13 (1) (2005) 3–16, http://dx.doi.org/10.1002/pip.556.

[9] L. Duan, H. Yi, C. Xu, M.B. Upama, M.A. Mahmud, D. Wang, F.H. Shabab, A. Uddin, Relationship between the diode ideality factor and the Carrier recombination resistance in organic solar cells, IEEE J. Photovolt. 8 (6) (2018) 1701–1709, http://dx.doi.org/10.1109/JPHOTOV.2018.2870722.
[10] A.A. Istratov, H. Hieslmair, E. Weber, Iron and its complexes in silicon, Appl. Phys. A 69 (1) (1999) 13–44, http://dx.doi.org/10.1007/s003390050968.
[11] J. Schmidt, Effect of dissociation of iron–boron pairs in crystalline silicon on solar cell properties, Prog. Photovolt., Res. Appl. 13 (4) (2005) 325–331, http://dx.doi.org/10.1002/pip.594.
[12] H. Zhu, X. Yu, X. Zhu, Y. Wu, J. He, J. Vanhellemont, D. Yang, Low temperature iron gettering by grown-in defects in p–type Czochralski silicon, Superlattices Microstruct. 99 (2016) 192–196, http://dx.doi.org/10.1016/j.spmi.2016.03.006.
[13] M. Burgelman, P. Nollet, S. Degrave, Modelling polycrystalline semiconductor solar cells, Thin Solid Films 361–362 (2000) 527–532, http://dx.doi.org/10.1016/S0040-6090(99)00825-1.
[14] K. Decock, S. Khelifi, M. Burgelman, Modelling multivalent defects in thin film solar cells, Thin Solid Films 519 (21) (2011) 7481–7484, http://dx.doi.org/10.1016/j.tsf.2010.12.039.
[15] M. Cappelletti, G. Casas, A. Cédola, E.P. y Blancá, B.M. Soucase, Study of the reverse saturation current and series resistance of p-p-n perovskite solar cells using the single and double-diode models, Superlattices Microstruct. 123 (2018) 338–348, http://dx.doi.org/10.1016/j.spmi.2018.09.023.
[16] M. Mostefaoui, H. Mazari, S. Khelifi, A. Bouraiou, R. Dabou, Simulation of high efficiency CIGS solar cells with SCAPS–1d software, Energy Procedia 74 (2015) 736–744, http://dx.doi.org/10.1016/j.egypro.2015.07.809.
[17] C.-H. Huang, W.-J. Chuang, Dependence of performance parameters of CdTe solar cells on semiconductor properties studied by using SCAPS–1d, Vacuum 118 (2015) 32–37, http://dx.doi.org/10.1016/j.vacuum.2015.03.008.
[18] F. Azri, A. Meftah, N. Sengouga, A. Meftah, Electron and hole transport layers optimization by numerical simulation of a perovskite solar cell, Sol. Energy 181 (2019) 372–378, http://dx.doi.org/10.1016/j.solener.2019.02.017.
[19] A. Hamache, N. Sengouga, A. Meftah, M. Henini, Modeling the effect of 1 MeV electron irradiation on the performance of n^+–p–p^+ silicon space solar cells, Radiat. Phys. Chem. 123 (2016) 103–108, http://dx.doi.org/10.1016/j.radphyschem.2016.02.025.
[20] E. Hu, G. Yue, R. Zhang, Y. Zheng, L. Chen, S. Wang, Numerical simulations of multilevel impurity photovoltaic effect in the sulfur doped crystalline silicon, Renew. Energy 77 (2015) 442–446, http://dx.doi.org/10.1016/j.renene.2014.12.049.
[21] B. Zhao, J. Zhou, Y. Chen, Numerical simulation of the impurity photovoltaic effect in silicon solar cells doped with thallium, Physica B 405 (18) (2010) 3834–3837, http://dx.doi.org/10.1016/j.physb.2010.06.012.
[22] A. McEvoy, T. Markvart, L. Castaner (Eds.), Solar Cells. Materials, Manufacture and Operation, second ed., Academic Press, Oxford, 2013.
[23] Z. Zhou, I. Perez-Wurfl, B.J. Simonds, Rapid, deep dopant diffusion in crystalline silicon by laser–induced surface melting, Mater. Sci. Semicond. Process. 86 (2018) 8–17, http://dx.doi.org/10.1016/j.mssp.2018.06.012.
[24] M.A. Green, Intrinsic concentration, effective densities of states, and effective mass in silicon, J. Appl. Phys. 67 (6) (1990) 2944–2954, http://dx.doi.org/10.1063/1.345414.
[25] S. Rein, S.W. Glunz, Electronic properties of interstitial iron and iron-boron pairs determined by means of advanced lifetime spectroscopy, J. Appl. Phys. 98 (11) (2005) 113711, http://dx.doi.org/10.1063/1.2106017.
[26] J.D. Murphy, K. Bothe, M. Olmo, V.V. Voronkov, R.J. Falster, The effect of oxide precipitates on minority carrier lifetime in p–type silicon, J. Appl. Phys. 110 (5) (2011) 053713, http://dx.doi.org/10.1063/1.3632067.
[27] T. Nærland, S. Bernardini, N. Stoddard, E. Good, A. Augusto, M. Bertoni, Comparison of iron-related recombination centers in boron, gallium, and indium doped silicon analyzed by defect parameter contour mapping, Energy Procedia 124 (2017) 138–145, http://dx.doi.org/10.1016/j.egypro.2017.09.321.
[28] S. Sakauchi, M. Suezawa, K. Sumino, H. Nakashima, Recombination–enhanced Fe atom jump between the first and the second neighbor site of Fe–acceptor pair in Si, J. Appl. Phys. 80 (11) (1996) 6198–6203, http://dx.doi.org/10.1063/1.363695.
[29] W. Wijaranakula, The reaction kinetics of iron–boron pair formation and dissociation in p–type silicon, J. Electrochem. Soc. 140 (1) (1993) 275–281, http://dx.doi.org/10.1149/1.2056102.
[30] H. Kohno, H. Hieslmair, A.A. Istratov, E.R. Weber, Temperature dependence of the iron donor level in silicon at device processing temperatures, Appl. Phys. Lett. 76 (19) (2000) 2734–2736, http://dx.doi.org/10.1063/1.126459.
[31] O. Breitenstein, Understanding the current-voltage characteristics of industrial crystalline silicon solar cells by considering inhomogeneous current distributions, Opto–Electron. Rev. 21 (3) (2013) 259–282, http://dx.doi.org/10.2478/s11772-013-0095-5.
[32] J. Sun, Q. Zhang, E.P. Tsang, DE/EDA: A new evolutionary algorithm for global optimization, Inform. Sci. 169 (3–4) (2005) 249–262, http://dx.doi.org/10.1016/j.ins.2004.06.009.
[33] K. Wang, M. Ye, Parameter determination of Schottky–barrier diode model using differential evolution, Solid-State Electron. 53 (2) (2009) 234–240, http://dx.doi.org/10.1016/j.sse.2008.11.010.
[34] L. Tong, M. Dong, C. Jing, An improved multi–population ensemble differential evolution, Neurocomputing 290 (2018) 130–147, http://dx.doi.org/10.1016/j.neucom.2018.02.038.
[35] M.U. Siddiqui, A. Arif, L. Kelley, S. Dubowsky, Three–dimensional thermal modeling of a photovoltaic module under varying conditions, Sol. Energy 86 (9) (2012) 2620–2631, http://dx.doi.org/10.1016/j.solener.2012.05.034.